Research on Dry Microwave Heating Infectious Aerosols or Droplets on Respirators

Kama Huang, *Senior Member, IEEE*, Junjun Li, and Yi Zhang, *Member, IEEE*

***Abstract*— Dramatic shortages of filtering facepiece respirator supplies generally occur following the outbreak of a pandemic such as COVID-19. Here, the decontamination and reuse of respirators are considered. Among decontamination methods, microwave irradiation has great potential because of easy access of microwave ovens. However, can a respirator be heated in a microwave oven for a certain time and then be reused? Herein, we demonstrate that dry microwave irradiation cannot heat infectious aerosols or droplets up to their deactivation temperature. The microwave absorption performance of a single aerosol or droplet was analyzed theoretically. The multiphysics simulation results indicate that a single aerosol or droplet can be barely heated under dry microwave irradiation. Experiments were carried out using a traveling wave system to verify the simulation. Following this, we simulated multiple aerosols and droplets on a respirator material, with the results indicating that the aerosols and droplets were at the same temperature as that of the respirator. Experimental measurements using a microwave oven demonstrated that the temperature increase of an N95 respirator under dry heating is less than 10 °C, which is far less than the temperature required to deactivate the COVID-19 virus. Although dry microwave heating cannot be used to heat the aerosols or droplets, microwave-generated steam has proved effective in deactivating infectious biological organisms. Therefore, to successfully decontaminate a used respirator in a microwave oven, a reservoir with a small amount of water beneath the respirator (or a steam bag to accommodate it) is essential to the decontamination process.**

***Index Terms*— Aerosols, COVID-19, droplets, microwave, respirator decontamination.**

I. Introduction

THE sudden emergence of respiratory infectious diseases, such as the unprecedented coronavirus disease of 2019 (COVID-19), generally leads to an international shortage of filtering facepiece respirator (FFR) supplies, which are essential for infection control and the protection of healthcare workers [1], [2]. Here, the decontamination and reuse of respirators, while suboptimal, can be considered [3]–[6]. Recent guidelines based on laboratory evidence that were proposed by the Infectious Diseases Society of America has recommend the use of a reprocessed N95 respirator for reuse during respirator shortage [6], [7]. A number of decontamination methods, including chemical solution treatment, oven heating, autoclaving, microwave irradiation, and ultraviolet germicidal irradiation (UVGI), have been researched and evaluated [1]–[6]. In 2020, Liao *et al.* [1] compared several decontamination methods and found that heat was the most promising nondestructive method for the preservation of filtration properties, whereas the solution-based method (e.g., ethanol or a chlorine-based solution) drastically degrades the filtration efficiency to unacceptable levels. Meanwhile, autoclaving is likely to result in physical damage of the FFRs [5]; although UVGI is a useful disinfection technique, the exact exposure or intensity of the UV light influence on the mask surface must be verified [1]. The UVGI treatments may also lead to improper fitting problems [8]. Later in 2020, decontamination methods using direct heating and microwave heating were systematically reviewed by Gertsman *et al.* [9] with the summary of the reported outcomes indicating that moist/dry microwave irradiation and moist/dry heating between 60 °C and 90 °C can maintain the fitting and functioning of the respirator. The moist microwave irradiation and moist/dry heat methods can be used to effectively deactivate viral pathogens on FFRs, whereas the germicidal effect of dry microwave irradiation has, as yet, not been reported [9].

Compared with other decontamination methods, microwave-based intervention for respirators has great potential because it presents the least time-intensive method and utilizes items commonly available in most households, cafeterias, restaurants, hospitals, and even research buildings [3], [10]. The decontamination of FFRs through microwaving was initiated more than 10 years ago. In 2007, Viscusi *et al.* [11] reported that dry microwave heating for 2 min did not result in a dramatic increase in penetration, and the inactivation of infectious biological organisms was not tested or evaluated [11]. Then, in 2011, Heimbuch *et al.* [12] found that more than $4\log_{10}$ reduction of a viable H1N1 virus could be achieved with six contaminated FFR models exposed to microwave-generated steam (MGS) for 2 min. Elsewhere, Fisher *et al.* [10] tested steam bags (which are typically used to decontaminate breast pump and infant feeding accessories) for the microwave decontamination of FFRs and found that they were 99.9% effective for inactivating bacteriophage MS2 on the apparatus, with the filtration efficiency remaining above 95% follow-

Manuscript received January 13, 2021; revised March 19, 2021 and April 23, 2021; accepted May 11, 2021. Date of publication June 18, 2021; date of current version September 2, 2021. This work was supported in part by the National Natural Science Foundation of China under Grant 61901286 and Grant 61731013, in part by the China Innovation Special Program of Science and Technology under Grant JG2019057, in part by the Open Project Funding of the Key Laboratory of Electromagnetic Wave Information Technology and Metrology of Zhejiang Province under Grant 2020KF0002, and in part by the Fundamental Research Funds for the Central Universities. *(Corresponding author: Yi Zhang.)*

The authors are with the College of Electronics and Information Engineering, Sichuan University, Chengdu 610064, China (e-mail: yizhang_ee@163.com).

Color versions of one or more figures in this article are available at https://doi.org/10.1109/TMTT.2021.3086539.

Digital Object Identifier 10.1109/TMTT.2021.3086539

ing decontamination. Later in 2012, Lore *et al.* [13] demonstrated that MGS can also effectively deactivate H5N1 on N95 respirators. Meanwhile, the investigation conducted by Bergman *et al.* [14] proved that decontamination processing using MGS does not result in significant degradation of the performance or physical integrity of N95 FFRs. In 2020, Zulauf *et al.* [3] described an MGS protocol for N95 respirators involving easy-access materials, including a glass container (to contain a small amount of water), a rubber band, and a household microwave oven.

Although the previous research indicates that microwave irradiation does not result in significant degradation to the filtering and fitting of the respirators, their successful decontamination must include deactivation of any present infectious biological organisms. However, in the previous reports, effective deactivation always involved a steam bag or a reservoir of water placed beneath the respirator within the microwave chamber [3], [10]. Thus, it remains unclear as to whether dry microwave treatment can directly deactivate the infectious biological organisms in the aerosols or droplets [14], [15]. Therefore, it is of great importance to determine (and note the broad masses of people) whether a reservoir of water/a steam bag is essential to the decontamination of respirators through microwaving. Since the contamination is mainly caused by viral aerosols and droplets with sizes ranging from 0.1 to 10 μm [16]–[18], the key to addressing the aforementioned issue lies in the following fundamental scientific question: Can microwaves directly heat these ultra-small particles? If not, placing water in the microwave chamber remains essential to the decontamination of FFRs. Most importantly, results for broad masses of people should be noted.

When microwave irradiates a dielectric material, scattering and absorption occur [19], [20], with the scattering and absorption performance varying according to the size of the heating sample. For example, as S. Barringer *et al.* [21] ascertained, oil samples heat up faster in a microwave oven than water samples of the same mass for a sufficiently large size, whereas the situation is reversed for very small samples. Another interesting phenomenon is that a bulk metal reflects microwave energy, whereas a powder metal absorbs it and can thus be heated fast [22]–[24]. Various other size-effect phenomena in microwave material processing were also discussed by Gamit and Chudasama [25]. To answer the aforementioned fundamental question, the scattering and absorption performance of an ultra-small water sphere, which represents an infectious aerosol or droplet, must first be determined.

In this article, we focus on the fundamental analysis of microwave heating of aerosols or droplets in an atmospheric pressure environment. An ultra-small water sphere with a size range of 0.1–10 μm was used to represent the infectious aerosol or droplet [16]–[18]. Mie theory and Rayleigh approximation were applied to calculate the dissipated microwave power in the ultra-small water sphere. Multiphysics simulation using COMSOL Multiphysics software was then applied to calculate the temperature increase of the sphere under microwave irradiation. Since microwave ovens from different manufacturers have different cavity sizes and microwave feeding locations, simulation using a specified microwave oven model may prevent generalization. Therefore, the microwave heating was modeled using a uniform plane microwave with an electric field strength of 6000 $\mathrm{V\cdot m^{-1}}$, which is higher than that of most microwave ovens [26], [27]. Tiny spheres of different sizes and dielectric properties were first modeled and analyzed to reveal the situation when a single aerosol or droplet was heated by microwave. To verify the simulation, we performed experiments involving a 3-D printed dielectric sphere with a size far smaller than the wavelength, which was placed in a traveling waveguide system. Following this, we modeled and simulated multiple hemispheres on the respirator materials to demonstrate the microwave heating performance of aerosols and droplets on a respirator. The temperature profile of a N95 respirator heated in a microwave oven for 2 min was also measured to illustrate the final temperature increase.

II. Microwave Heating a Single Aerosol or Droplet

A. Theoretical Derivation

Without loss of generality, a sphere with radius r_d is placed in air. When uniform plane microwaves radiate to the sphere, scattering, and absorption occur. Therefore, the field at any point outside the sphere is the sum of the primary and diffracted field by the sphere. The resultant field can be written as [19]

$$\vec{E} = \overrightarrow{E}_i + \overrightarrow{E}_r \tag{1a}$$

$$\vec{H} = \overrightarrow{H}_i + \overrightarrow{H}_r \tag{1b}$$

where $\vec{E}$ and $\vec{H}$ are the resultant electric and magnetic field, respectively, and the subscripts i and r indicate the primary and diffracted wave, respectively.

If a concentric spherical surface (with radius R) was drawn outside the sphere, then, the radial component of the total complex flow vector can be written as [19]

$$S_R = \frac{1}{2}\left(E_\theta H_\phi^* - E_\phi H_\theta^*\right) \tag{2}$$

where S_R is the Poynting vector in the regions with radius R, and the subscripts θ and ϕ indicate the direction in the spherical coordinate frame, the superscript $*$ indicates conjugate. Taken (1) into (2), we can get

$$\begin{aligned} S_R = {} & \frac{1}{2}\left(E_{i\theta} H_{i\phi}^* - E_{i\phi} H_{i\theta}^*\right) + \frac{1}{2}\left(E_{r\theta} H_{r\phi}^* - E_{r\phi} H_{r\theta}^*\right) \\ & + \frac{1}{2}\left(E_{i\theta} H_{r\phi}^* + E_{r\theta} H_{i\phi}^* - E_{i\phi} H_{r\theta}^* - E_{r\phi} H_{i\theta}^*\right). \end{aligned} \tag{3}$$

When energy is converted into heat within the sphere, the net flow is equal to the amount of absorbed energy and is directed inward. Thus, the total energy absorbed by the sphere can be written as

$$P_a = -\mathrm{Re}\int_0^{\pi}\int_0^{2\pi} S_R R^2 \sin\theta d\phi d\theta. \tag{4}$$

Take (3) into (4) we can get

$$P_a = -\frac{1}{2}\mathrm{Re}\int_0^{\pi}\int_0^{2\pi}\left(E_{i\theta}H_{i\phi}^* - E_{i\phi}H_{i\theta}^*\right)R^2\sin\theta d\phi d\theta - \frac{1}{2}\mathrm{Re}\int_0^{\pi}\int_0^{2\pi}\left(E_{r\theta}H_{r\phi}^* - E_{r\phi}H_{r\theta}^*\right)R^2\sin\theta d\phi d\theta - \frac{1}{2}\mathrm{Re}\int_0^{\pi}\int_0^{2\pi}\left(E_{i\theta}H_{r\phi}^* + E_{r\theta}H_{i\phi}^* - E_{i\phi}H_{r\theta}^* - E_{r\phi}H_{i\theta}^*\right) \times R^2\sin\theta d\phi d\theta. \quad (5)$$

The first term on the right side of (5) equals 0 since the first term on the right side of (3) measures the flow of energy in the incident wave [19]. The negative of the second term on the right side of (5) is the scattered power which can be written as

$$P_s = \frac{1}{2}\mathrm{Re}\int_0^{\pi}\int_0^{2\pi}\left(E_{r\theta}H_{r\phi}^* - E_{r\phi}H_{r\theta}^*\right)R^2\sin\theta d\phi d\theta. \quad (6)$$

Then, let us represent the last term of (5) as P_t which can be written as

$$P_t = -\frac{1}{2}\mathrm{Re}\int_0^{\pi}\int_0^{2\pi}\left(E_{i\theta}H_{r\phi}^* + E_{r\theta}H_{i\phi}^* - E_{i\phi}H_{r\theta}^* - E_{r\phi}H_{i\theta}^*\right) \times R^2\sin\theta d\phi d\theta. \quad (7)$$

Based on (5)–(7), the absorbed microwave power (P_a) can be calculated by the following equation:

$$P_a = P_t - P_s. \quad (8)$$

Here, P_t and P_s can be calculated by allowing R to grow very large and introducing the asymptotic values of the spherical Bessel function and spherical Hankel function of the first kind. The details of the derivation were demonstrated in [19]. Then, P_t and P_s can be calculated using the following equations:

$$P_t = \pi\frac{E_0^2}{k_{\mathrm{air}}^2}\sqrt{\frac{\varepsilon_0}{\mu_0}}\mathrm{Re}\sum_{n=1}^{\infty}(2n+1)(a_n+b_n) \quad (9)$$

and

$$P_s = \pi\frac{E_0^2}{k_{\mathrm{air}}^2}\sqrt{\frac{\varepsilon_0}{\mu_0}}\sum_{n=1}^{\infty}(2n+1)\left(|a_n|^2+|b_n|^2\right) \quad (10)$$

where E_0 is the electric field amplitude of the primary incident wave, ω is the frequency of the incident microwave, k_{air} is the wavenumber in air and can be calculated by $(\varepsilon_0\mu_0)^{1/2}$, and ε_0 and μ_0 are the permittivity and permeability of air, respectively. Here, a_n and b_n can be calculated using the following equations [19], [28]:

$$a_n = -\frac{\mu_d j_n(Nx)[xj_n(x)]' - j_n(x)[Nxj_n(Nx)]'}{\mu_d j_n(Nx)\left[xh_n^{(1)}(x)\right]' - h_n^{(1)}(x)[Nxj_n(Nx)]'} \quad (11)$$

and

$$b_n = -\frac{\mu_d j_n(x)[Nxj_n(Nx)]' - N^2 j_n(Nx)[xj_n(x)]'}{\mu_d h_n^{(1)}(x)[Nxj_n(Nx)]' - N^2 j_n(Nx)\left[xh_n^{(1)}(x)\right]'} \quad (12)$$

where N is the complex refractive index, which can be calculated by $(\varepsilon_d\mu_d)^{1/2}$; ε_d and μ_d are the relative permittivity and permeability of the dielectric sphere, respectively; $x = (2\pi r_d)/\lambda$ is the size parameter; and $j_n(x)$ and $h_n^{(1)}(x)$ denote the spherical Bessel function and the spherical Hankel function of the first kind, respectively [19], [28].

For a nonmagnetic dielectric sphere, $\mu_d = 1$. If $x \ll 1$, Rayleigh approximation can be applied, and only the first-order electric oscillation needs to be taken into account. Then, (9) and (10) can be approximated as follows [19]:

$$P_t \approx \frac{3\pi E_0^2}{k_{\mathrm{air}}^2}\sqrt{\frac{\varepsilon_0}{\mu_0}}\mathrm{Re}(b_1) \quad (13)$$

and

$$P_s \approx \frac{3\pi E_0^2}{k_{\mathrm{air}}^2}\sqrt{\frac{\varepsilon_0}{\mu_0}}\left(|b_1|^2\right). \quad (14)$$

The amplitude of the first-order electric oscillation (b_1) can be approximately calculated using the following equation [19]:

$$b_1 \approx -\frac{2i\left(N^2-1\right)}{3\left(N^2+2\right)}x^3. \quad (15)$$

For a dielectric sphere, its complex relative permittivity can be expressed as follows [19]:

$$\varepsilon_d = \varepsilon_d' + i\varepsilon_d''. \quad (16)$$

Thus, b_1 can be expressed as

$$b_1 = \frac{2\varepsilon_d''}{\left(\varepsilon_d'+2\right)^2+\varepsilon_d''^2}x^3 - \frac{2i\left(\varepsilon_d'^2+\varepsilon_d''^2+\varepsilon_d'-2\right)}{3\left(\varepsilon_d'+2\right)^2+3\varepsilon_d''^2}x^3. \quad (17)$$

Substituting (13), (14), and (17) into (8), we can obtain

$$P_a \approx \frac{6\pi\sqrt{\varepsilon}_0\varepsilon_d''E_0^2}{k_{\mathrm{air}}^2\sqrt{\mu}_0\left[\left(\varepsilon_d'+2\right)^2+\varepsilon_d''^2\right]}x^3. \quad (18)$$

In microwave heating, the absorbed microwave power of the materials is generally transferred into heat, the transport equation of which can be expressed as follows [22], [29]:

$$\rho_d C_d\frac{\partial T}{\partial t} - \nabla\cdot(k_{\mathrm{tc}}\nabla T) = P_{\mathrm{uv}} \quad (19)$$

where ρ_d, C_d, and k_{tc} denote the material density, heat capacity, and thermal conductivity, respectively; T is temperature; and P_{uv} is the microwave power dissipated per unit volume. When the dielectric sphere is extremely small, the dissipated microwave power and temperature in the sphere can be approximated to uniform distribution [22]. Thus, P_{uv} can be calculated by P_a/V_m, where V_m is the volume of the sphere.

Here, let us first assume that there is no thermal exchange between the sample and its surrounding atmosphere. Then, the temperature increase can be expressed as follows:

$$\Delta T = \frac{9\pi\sqrt{\varepsilon}_0\varepsilon_d''E_0^2}{\rho_d C_d\lambda\sqrt{\mu}_0\left[\left(\varepsilon_d'+2\right)^2+\varepsilon_d''^2\right]}t. \quad (20)$$

An interesting point that emerges from (20) is that the temperature increase of the ultra-small dielectric sphere is not related to its size if no thermal exchange takes place. This result is consistent with that of a previous analysis. In 2009, Moosmuller and Arnott [30] demonstrated that the absorption cross section of an ultra-small sphere is proportional to r^3,

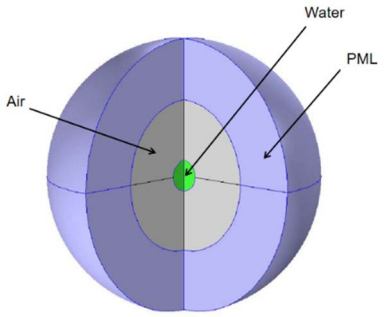

Fig. 1. Multiphysics simulation model of an ultra-small water sphere (which represents a single aerosol or droplet) heated in a uniform plane microwave.

whereas the required power to heat a material to a specific temperature is also proportional to its volume, which can be calculated using $(4r^3)/3$ for a sphere, under thermal isolation conditions. Thus, the temperature increase of an ultra-small sphere under thermal isolation conditions is only related to the microwave field intensity, the wavelength, and the dielectric and thermal properties of the material, as well as the heating period. Interestingly, the temperature increase is independent of the size of the sphere.

In practice, thermal convection and emission occur if the material's temperature is higher than that of its surroundings, with the thermal emission being weak and ignorable if the temperature difference is not dramatic [29]. To obtain the realistic temperature increase, multiphysics simulation could be conducted under the convective heat transfer boundary condition, which was specified as follows [22], [29]:

$$h(T - T_{\text{air}}) = n \cdot (k_{\text{tc}} \Delta T) \tag{21}$$

where h is the convection heat transfer coefficient, and T_{air} is the temperature of the surrounding air. With the dissipated microwave power (18), the heat transport equation (19) and the boundary condition (21), the microwave heating performance could be simulated and analyzed, as demonstrated in Section II-B.

B. Modeling, Simulation, and Discussion of Microwave Heating a Single Aerosol or Droplet

Without loss of generality, a multiphysics simulation model of an ultra-small water sphere in a uniform plane microwave with frequency of 2.45 GHz was built, as illustrated in Fig. 1. The water sphere at the center represents an aerosol or a droplet. The surrounding environment is air with initial temperature and thermal conductivity of 20 °C and 0.0258 $\text{W} \cdot \text{m}^{-1} \cdot \text{K}^{-1}$, respectively. The convective heat transfer coefficient at the surface of the water sphere was set to be 6 $\text{W} \cdot \text{m}^{-1} \cdot \text{K}^{-1}$ [31]. The uniform plane microwave was set as the background electromagnetic wave with an electric field strength of 6000 $\text{V} \cdot \text{m}^{-1}$, which is higher than that in most microwave ovens [26], [27]. The whole structure was covered by a perfect matching layer (PML) to simulate an infinite space [32]. The parameters of the water, the respirator, and the 3-D printing material in the simulation are presented in Table I [21], [33].

TABLE I
MATERIALS' PARAMETERS USED IN SIMULATION

Parameters	Distilled water	Respirator (polypropylene)	3D printed sphere
ε_d'	77.4	1.599	3
ε_d''	9.48	0.07	0.003
k_{tc} $(W \cdot m^{-1}K^{-1})$	0.609	0.22	0.25
ρ_d $(kg \cdot m^{-3})$	1000	900	1160
C_d $(J \cdot kg^{-1}K^{-1})$	4190	1900	1000

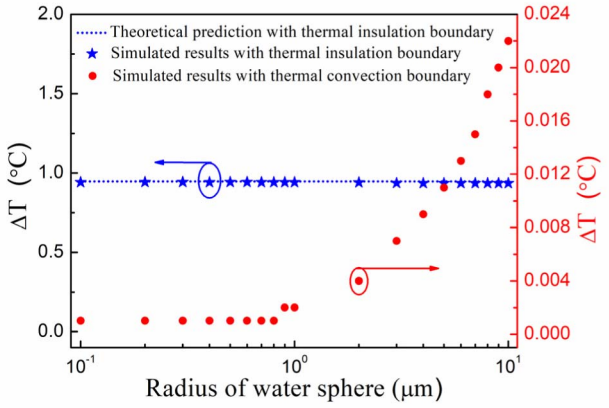

Fig. 2. Temperature increase of the spheres with different sizes after heating for 2 min.

In the simulation, the diameter of the water sphere was changed between 0.1 and 10 μm, which is the size range of the infectious aerosols and droplets [16]–[18]. The heating time was set to 2 min in line with most of the previously reported experiments [11]–[15]. After 2 min of heating, the final temperatures of the spheres with different sizes under different thermal boundary conditions were obtained, as illustrated in Fig. 2. The boundary condition of thermal insulation was applied in the simulation to verify the theoretical prediction, whereas the boundary condition of thermal convection was applied to simulate a realistic situation.

As Fig. 2 indicates, the theoretical temperature increase calculated from (20) was 0.948 °C. The simulated results under the thermal insulation boundary condition matched the theoretical predictions well. However, in the realistic situation (with the thermal convection boundary condition), the temperature increase was far smaller than that under the ideal thermal insulation condition. The highest temperature increase was only 0.022 °C for the sphere with a radius of 10 μm, whereas with a decrease in sphere radius, the temperature increase became even lower. When the radius of the sphere was less than 0.2 μm, a temperature increase could barely be observed.

In Fig. 2, the distilled water was used as the sample material. But realistically, saliva from different individuals may possess distinctive permittivity [34], thus affecting the heating performance. Here, the heating results of sphere samples with different dielectric properties were compared in Table II [34], [35]. Notably, ΔT increases with the increasing of material's loss tangent. The increasing of ΔT under thermal insulation

TABLE II
TEMPERATURE INCREASE (ΔT) OF DIFFERENT SAMPLE MATERIALS AFTER MICROWAVE HEATING FOR 2 min

Sample materials	ε'_d	Loss tangent	Radius of the Sphere (μm)	Simulated ΔT under thermal insulation condition (°C)	Simulated ΔT under thermal convection condition (°C)
Distilled water	77.4	0.122	0.1	0.94	0.001
			1	0.94	0.002
			10	0.94	0.022
Saliva from different individuals	69.7	0.145	0.1	1.23	0.001
			1	1.23	0.002
			10	1.23	0.024
	68.9	0.153	0.1	1.31	0.001
			1	1.31	0.003
			10	1.31	0.025
	71.6	0.153	0.1	1.31	0.001
			1	1.31	0.003
			10	1.31	0.025
Sea water	65.5	0.502	0.1	3.72	0.004
			1	3.72	0.007
			10	3.72	0.072

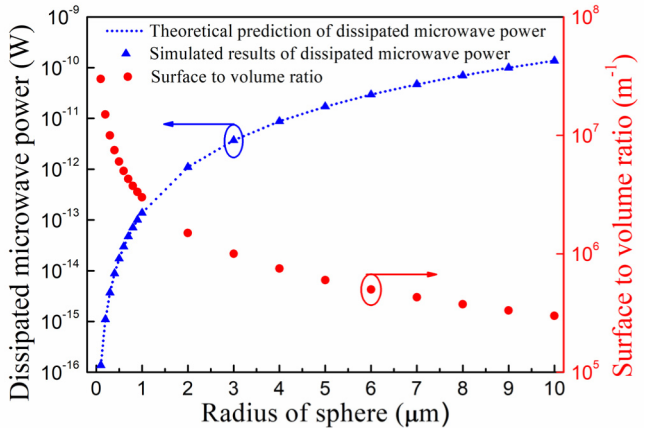

Fig. 3. Dissipated microwave power and the surface to volume ratio of spheres with different sizes.

condition is more evident than that under thermal convection condition, which indicating that thermal convection narrows the temperature difference caused by the distinctive loss tangent of materials in microwave heating ultra-small samples. Under thermal convection condition, the variation of ΔT was more significant with larger sample size, while the sample with very small size did not show obvious temperature difference, though the loss tangent of the sample's material increased in the same manner.

To explain the heating results illustrated in Fig. 2 and Table II, the dissipated microwave power and the surface to volume ratio of the spheres (with sample material using distilled water) were determined, as illustrated in Fig. 3. Although the sphere with a larger size absorbed more microwave energy, the higher mass consumed more energy in reaching the same temperature. Consequently, when the thermal exchange with the surrounding environment was ignored, the temperature was the same for spheres of different sizes, as was predicted by (20), provided the Rayleigh approximation was satisfied.

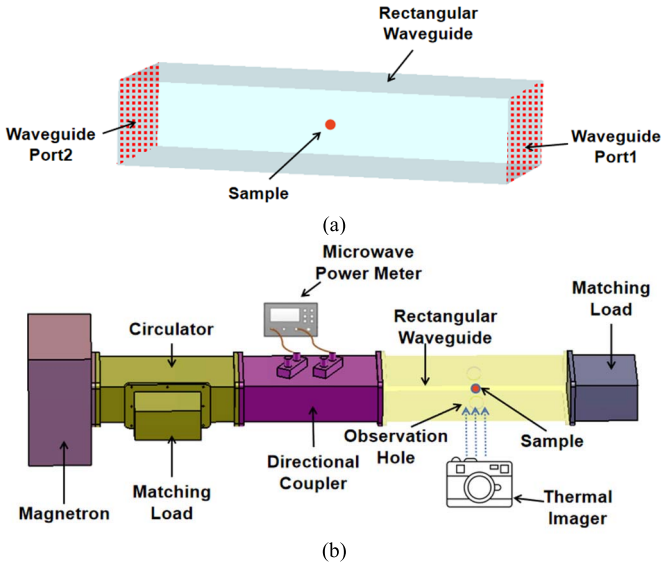

Fig. 4. Verification of the multiphysics simulation with a traveling wave system. (a) Simulation model of an ultra-small sphere heated in a waveguide and (b) experimental verification system with a WR340 waveguide system.

However, in the realistic situation, the thermal convection strongly affected the heating process, especially when the size of the sample was extremely small. The large values of surface to volume ratio of the small samples result in extremely strong thermal exchange between the sample and its surrounding air. As illustrated in Fig. 3, the surface to volume ratio reached 3×10^5 m^{-1} when the sphere radius was 10 μm, with the value increasing more dramatically as the size of the sphere was reduced. The high surface to volume ratio values resulted in that it was difficult to heat the ultra-small samples in the microwave.

C. Experimental Verification

To verify the multiphysics simulation, further experiments were carried out. The very strong sensitivity of the electric field exerted on a dielectric object on its position and its dielectric nature in a multimode cavity does not allow a quantitative investigation in a microwave oven. To circumvent this issue, we built a traveling wave system with WR340 waveguides, with the experimental system and simulation model illustrated in Fig. 4. During the simulation, waveguide ports were applied at both ends of the waveguide to simulate the traveling microwave. Since a single sphere with a micrometer size is difficult to produce and handle, and the purpose of this experiment was to verify the validity of the multiphysics simulation rather than confirming that an ultra-small sphere can barely be heated by a microwave, a dielectric sphere with a radius of 1.5 mm produced using 3-D printing (Wenext Corporation) was placed in the middle of the waveguide cavity to be heated. Dielectric and thermal parameters of the sphere are listed in Table I.

A magnetron (Panasonic 2M244) was used as the microwave source in the experiments. This magnetron, which is used in many microwave ovens, can generate 1000 W of continuous microwave power, which is close to the power

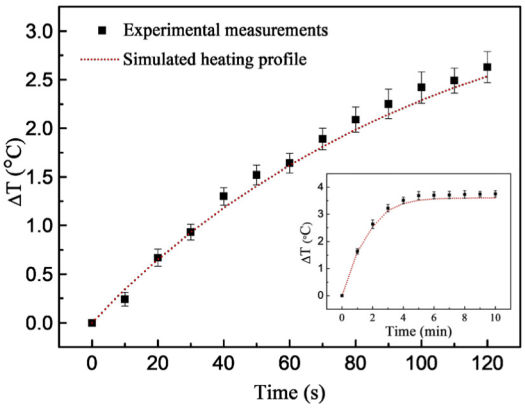

Fig. 5. Comparison of the simulated heating profile and the experimental measurements using the travelling waveguide system. The inserted subfigure depicts the simulated and experimental heating profile with a relatively long period.

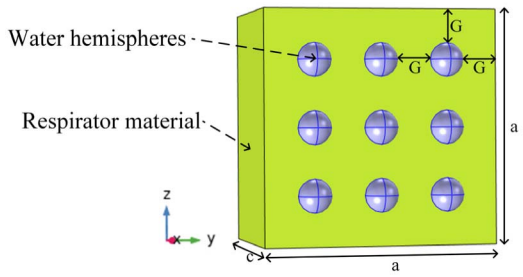

Fig. 6. Simulation model with water hemispheres attached on the respirator material (G represents the gap distance between two hemispheres, a and c represent the side length and thickness of the respirator material).

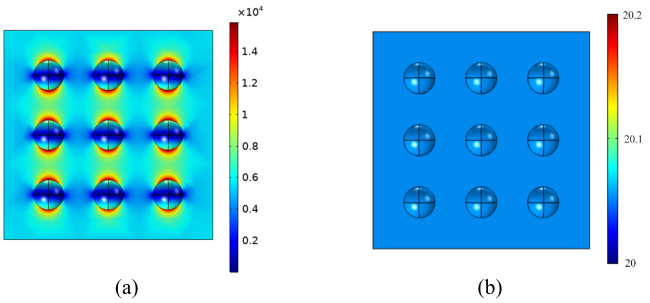

Fig. 7. (a) Electric field distribution in the respirator material and water hemispheres (unit: $\mathrm{V \cdot m^{-1}}$). (b) Surface temperature of the water hemispheres and the respirator material (unit: °C).

level of most microwave ovens. A circulator with a water load connected was applied to protect the microwave source, and a waveguide cavity with observation holes was used to place the sample. Another load was connected to the heating cavity to absorb the transmitted microwave, thus producing the traveling microwave situation. The load connected to the heating waveguide in experiments corresponds to a waveguide port in simulation. The temperature of the sphere was measured using a thermal imager (VarioCAM high resolution, InfraTec Corporation) in real time using the observation holes (with the cut-off structure connected).

The heating profiles of the simulation and the experiments are illustrated in Fig. 5. As the inserted subfigure indicates, the sphere experienced a relatively rapid temperature increase in the first 3 min before the heating rate slowed and the temperature approached an asymptotic line with thermal equilibrium. At the beginning of the heating period, there was almost no temperature difference between the sample and its surrounding air. The electromagnetic energy transferred to heat in the sample directly, which caused high heating rate. As the heating process went on, the thermal exchange between the sample and its surrounding air became significant due to the enlarged temperature difference, which slowed down the heating rate. As the temperature difference got larger and larger, thermal equilibrium finally reached. Notably from Fig. 5, the simulated results were almost in line with the experimental measurements. At the final stage of heating, the temperature in simulation is a little bit (around 0.15 °C) lower than that from experimental measurements. The main reason for this phenomenon should be that the heat generated on the walls of the waveguide by the surface current and the temperature increase of the line which hung the sphere were not considered in the simulation.

III. Microwave Heating of Multiple Aerosols and Droplets on Respirators

Following the study on microwave heating of a single aerosol or droplet, multiple aerosols and droplets on the N95 respirators were modeled and simulated to reveal the practical situations, with the model illustrated in Fig. 6. Here, a 3 × 3 array of water hemispheres was attached to a piece of a respirator material (polypropylene). The shape of water on the respirator material may vary depending on the model and layer of the respirator due to the change of the material's hydrophobicity and hydrophilia. Here, hemispheres were used for simplification. The length and width of the respirator material were set to be slightly larger than the size of the array (the distance from the edge of the array to the edge of the respirator material was set to be the same as the gap between two spheres). The whole simulated sample was emerged in a uniform plane microwave propagating in the $\overrightarrow{+x}$-direction with linear polarization of electric field along the $\vec{z}$-direction. The material of the surrounding environment is air, which forms a sphere outside the sample. And outside the big air sphere, PML was applied to simulate an infinite space. The side length and thickness of the respirator material were represented by a and c, which equals $(6r_d + 4G)$ and $10r_d$, respectively, with G representing the gap distance between two hemispheres.

First, the effect of the hemispheres radius (r_d) on the heating results was investigated. Here, the gap between each hemisphere (G) was fixed to equal the diameter of the hemisphere. Fig. 7 presents the simulated surface electric field strength and surface temperature of the hemispheres and the respirator, with a hemisphere radius of 1 μm, and the average volume temperature increase of the water hemispheres and the respirator, as well as the absorbed power and power density, are listed in Table III. From Fig. 7(a), it is clear that the electromagnetic

TABLE III

COMPARISON OF AVERAGE VOLUME TEMPERATURES, DISSIPATED POWER DENSITY, AND TOTAL DISSIPATED POWER OF THE HEMISPHERES AND THE RESPIRATOR MATERIAL WITH DIFFERENT SPHERE RADII

Radius of the hemisphere (μm)	Average volume temperature increase of hemispheres (°C)	Average volume temperature increase of the respirator material (°C)	Average dissipated power density in the water hemispheres ($W \cdot m^{-3}$)	Average dissipated power density in the respirator material ($W \cdot m^{-3}$)	Total dissipated power in the water hemispheres (W)	Total dissipated power in the respirator material (W)
0.5	0.02	0.02	1.38×10^5	1.26×10^5	3.26×10^{-13}	3.09×10^{-11}
1	0.04	0.04	1.38×10^5	1.26×10^5	2.61×10^{-12}	2.47×10^{-10}
5	0.21	0.21	1.38×10^5	1.26×10^5	3.26×10^{-10}	3.09×10^{-8}
10	0.51	0.51	1.38×10^5	1.26×10^5	2.60×10^{-9}	2.47×10^{-7}

field distribution around the hemisphere matched the first-order electric oscillation [19]. However, the temperature was uniformly distributed in all the hemispheres and the respirator. Meanwhile, as Table III indicates, the average dissipated power density in the hemispheres is usually a little bit higher than that in the respirator. Nevertheless, the respirator material absorbed much more total microwave power than the hemispheres since the volume of the respirator material is much larger than the collective volume of the hemispheres. Though the dissipated power density and total absorbed power are different between the respirator material and hemispheres, the temperature of the hemisphere was always equal to that of the respirator. The main reason for this was that the whole structure was still extremely small at less than 14 μm when the hemispheres radius was 1 μm. The thermal exchange between these ultra-small structures was so rapid that they reached the thermal equilibrium in an extremely short period of time. Once the hemispheres on the respirator material become large enough (larger than 1 mm), the temperature difference between the hemisphere and its connecting material would appear. Therefore, in the study here, the temperature was uniformly distributed across the whole structure in terms of different materials.

Moreover, the temperature increase of the structure with larger hemispheres was higher than that of the structure with smaller hemispheres because of the increase in size of the structure as a whole. By comparing the temperature increase illustrated in Fig. 2 with that in Table III, we can conclude that the temperature increase of multiple hemispheres is higher than that of a single sphere, again because of the increase in size of the entire structure with multiple hemispheres.

For the results presented in Table IV, the hemisphere radius was fixed at 1 μm, while the gap between the hemispheres was adjusted. The average dissipated power density varied with the gap of the hemispheres since the scattering of the hemispheres resulted in microwave field perturbation. But generally, the average dissipated power density in the hemispheres was a little bit higher than that in the respirator. But the temperature of the hemispheres and respirator material was still the same. When the gap became smaller, the temperature increase was reduced, which, again, was due to the size of the whole structure. As the hemispheres moved closer, the size of the whole structure was reduced.

Table V demonstrated the simulated results with different dielectric properties of the hemispheres, with radius and gap of the hemispheres fixed at 1 and 2 μm, respectively. Generally, the average dissipated power density increased with the increasing of material's loss tangent. The results are expectable since the materials with higher loss tangent usually show stronger microwave absorption. The total dissipated power in the hemispheres show the same variation trend with the dissipated power density since the size of the hemispheres is the same regarding different dielectric properties. However, the temperature increment of the hemispheres was the same, regarding different dielectric properties. The main reason is that the temperature of the hemispheres was always the same as that of the respirator material due to the ultra-fast thermal exchange.

In the above results, the temperature was uniformly distributed since the whole structure size was so small. In practical situations, the size of the respirator will be larger than the micrometer size. Therefore, we modeled the hemisphere array when attached to the central area of a comparatively large respirator material with size of 5 mm $\times$ 5 mm $\times$ 0.5 mm. Here, the radius and the positions of the hemispheres were randomly distributed to simulate actual aerosols and droplets on the respirator. The radius of the hemispheres was determined using a random number generation function. Other simulation conditions are same to the model in Fig. 6. The background microwave propagates in the $+\overrightarrow{x}$-direction with linear polarization of electric field along the $\vec{z}$-direction. The surrounding environment is an air sphere with PML outside the sphere. The simulated temperature distribution after heating is illustrated in Fig. 8. Here, the temperature was no longer uniformly distributed in the whole structure, as illustrated in Fig. 8(a). A higher temperature was observed in the central area, and the temperature at the fringes was lower since the thermal exchange in the fringe area was much stronger than that in the central area. The microwave electric field in the upper and lower fringes in Fig. 8(a) is also lower than that in the other areas, which also contributes to the temperature distribution after heating. The temperature inside the respirator material was also demonstrated with the thermal profile of the cut plane (*zox* plane), as shown in Fig. 8(b). Notably, the temperature anisotropy along thickness of the respirator material is not significant. When we zoomed in on the central area, we observed that the hemispheres shared the same temperature with the respirator material, as indicated in Fig. 8(c). Meanwhile, Fig. 8(d) illustrates electric field intensities in the central area. Although the randomly distributed hemispheres with random

TABLE IV

COMPARISON OF AVERAGE VOLUME TEMPERATURES, DISSIPATED POWER DENSITY, AND TOTAL DISSIPATED POWER OF HEMISPHERES AND THE RESPIRATOR MATERIAL WITH DIFFERENT SPHERE GAPS

Distance between two hemispheres (μm)	Average volume temperature increase of hemispheres (℃)	Average volume temperature increase of the respirator material (℃)	Average dissipated power density in the water hemispheres ($W \cdot m^{-3}$)	Average dissipated power density in the respirator material ($W \cdot m^{-3}$)	Total dissipated power in the water hemispheres (W)	Total dissipated power in the respirator material (W)
1	0.03	0.03	1.29×10^{5}	1.20×10^{5}	2.43×10^{-12}	1.20×10^{-10}
2	0.04	0.04	1.38×10^{5}	1.26×10^{5}	2.61×10^{-12}	2.47×10^{-10}
4	0.06	0.06	1.33×10^{5}	1.21×10^{5}	2.29×10^{-12}	6.46×10^{-10}

TABLE V

COMPARISON OF AVERAGE VOLUME TEMPERATURES, DISSIPATED POWER DENSITY, AND TOTAL DISSIPATED POWER OF THE RESPIRATOR MATERIAL AND HEMISPHERES WITH DIFFERENT DIELECTRIC PROPERTIES

Sample materials	ε'_d	Loss tangent	Average volume temperature increase of hemispheres (℃)	Average volume temperature increase of the respirator material (℃)	Average dissipated power density in the water hemispheres ($W \cdot m^{-3}$)	Average dissipated power density in the respirator material ($W \cdot m^{-3}$)	Total dissipated power in the water hemispheres (W)	Total dissipated power in the respirator material (W)
Distilled water	77.4	0.122	0.04	0.04	1.38×10^{5}	1.26×10^{5}	2.61×10^{-12}	2.47×10^{-10}
Saliva from different individuals	69.7	0.145	0.04	0.04	2.22×10^{5}	1.26×10^{5}	4.19×10^{-12}	2.47×10^{-10}
	68.9	0.153	0.04	0.04	2.44×10^{5}	1.26×10^{5}	4.59×10^{-12}	2.47×10^{-10}
	71.6	0.153	0.04	0.04	2.23×10^{5}	1.26×10^{5}	4.21×10^{-12}	2.47×10^{-10}
Sea water	65.5	0.502	0.04	0.04	5.46×10^{5}	1.26×10^{5}	1.03×10^{-11}	2.47×10^{-10}

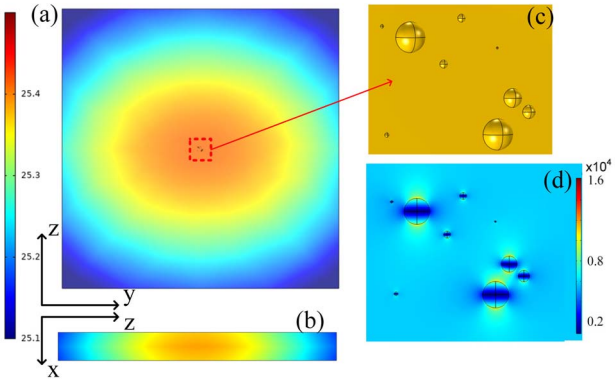

Fig. 8. Simulated results of nine hemispheres with random sizes distributed randomly on a piece of a relatively large respirator material. (a) and (b) Temperature distribution on the entire respirator material's surface and at the cut plane of the respirator material, respectively (unit: °C). (c) Surface temperature in the sphere area. (d) Microwave electric field distribution in the hemisphere area (unit: $V \cdot m^{-1}$).

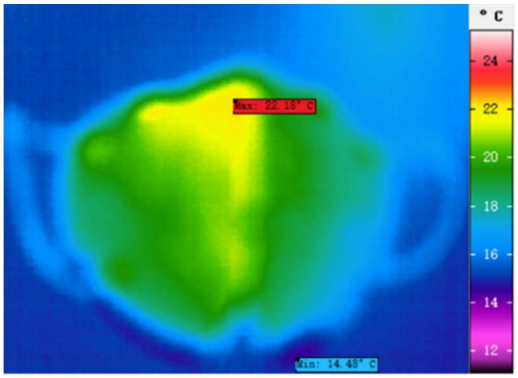

Fig. 9. Measured temperature of a N95 respirator heated in a microwave oven for 2 min (dry heating).

sizes resulted in nonuniform microwave field distribution, this did not result in a nonuniform final temperature distribution.

From the aforementioned results, we can conclude that the temperature of the water hemispheres was always the same as that of the respirator material, due to the rapid thermal exchange between them. We also carried out the simulation of microwave heating a whole respirator with a tiny water hemisphere on it in a microwave oven cavity. There is still no temperature difference between the hemisphere and the respirator material around it. Therefore, once the temperature of the respirator after dry microwave heating was measured, the temperature of the aerosols and droplets on it could be obtained. We thus heated a dry N95 mask in a microwave oven (Galanz G90F23CN3PV-BM1) for 2 min. The temperature of the entire respirator was measured immediately using the thermal imager, with the results illustrated in Fig. 9. Here, the colored central area is the temperature of the respirator, and the surrounding area represents the temperature of the lab table. Notably, the maximum measured temperature of the respirator was 22.18 °C, and that of the surrounding environment was 14.48 °C. The experiments were repeated three times, with the maximum temperature increase of the respirator being less than 10 °C on each occasion. According to our analysis, the aerosols and droplets on the respirator and the respirator itself were at the same temperature. Thus, the temperature increase of the infectious aerosols or droplets was also less than 10 °C, which is far lower than the temperature required to deactivate the COVID-19 virus (>70 °C) [1], [11]. The analytical results here are in very good agreement with the experimental results obtained by Zulauf *et al.* [3]. In their experiments, the respirator segments on a mug (with water inside) exhibited a $<4\log_{10}$ reduction in plaque-forming units (PFUs), whereas the elastic straps draped over the edges of the mug exhibited only a $1–3\log_{10}$ reduction in PFUs. Although

the elastic straps were irradiated by microwave, it cannot reach the safe decontamination level for reuse due to the minimal exposure to the generated steam [3]. This significant decrease demonstrated that dry microwave irradiation cannot be used to decontaminate a respirator to a safe level for reuse.

To deactivate the COVID-19 virus on a respirator through microwave heating, the inclusion of water under the entire respirator is essential. In addition to the reasons discussed earlier, without water, which is a strong absorption material for microwaves, the electric field intensity in the cavity would be fairly high. Thus, arcing damage is more likely to occur at the wire nose-bridges of a number of respirator models, especially those with metal nose strips [1], [15]. Furthermore, as Li *et al.* [36] emphasized, humidity plays an important role in the decontamination of respirators through heat. In short, the inclusion of water in the microwave oven is essential, but the volume of water should not be too large. In the experiments carried out by Pascoe *et al.* [37], the volume of water under the respirator affected the required time for the MGS decontamination. By increasing the water volume from 100 to 200 mL, the time to attain a $6\log_{10}$ reduction of *Staphylococcus aureus* on the respirator was increased from 60 to 90 s.

From the foregoing analysis, it would appear that the correct volume of water in the decontamination process using the MGS method remains unclear. Pascoe *et al.* [37] used volumes of 200 and 100 mL; Zulauf *et al.* [3] used a volume of 60 mL; both Lore *et al.* [13] and Bergman *et al.* [14] used a 50-mL volume of room-temperature tap water; and other water volumes are likely to be found in other published reports. Here, we believe that there is no need to be precise on the volume of water because this may vary depending on the model of a microwave oven, with different models having differing power or cavity size. However, a number of basic principles can be suggested to help determine the volume of water in MGS decontamination. First, the water should be present in the whole processing period because the generated steam works for the decontamination and the absence of water will likely result in arcing. Second, the volume of water should not be too large because a higher volume of water will slow the temperature increase and reduce the generated steam. Third, if arcing does occur in the decontamination process, increasing the water volume may be a solution, albeit the respirator may need to be processed for a slightly longer period. Last, and perhaps most importantly, the reservoir beneath the respirator should be large enough to incorporate the entire respirator, including the straps.

Another interesting point of note is that the microwave heating of aerosols and droplets on a contaminated respirator is different from that involving a compressed powder sample, even though both have a basic composition of ultra-small particles. For the contaminated respirator, the aerosols and droplets will likely be randomly distributed on and in the respirator, whereas for the compressed powder sample, the particles will be compactly connected because the collective particles will be compressed under high pressure (typically 300–900 MPa) [38]. In terms of the randomly distributed aerosols and droplets, each element may undergo strong thermal exchange with its surrounding air and the respirator material, whereas in terms of the compactly compressed sample, most of the particles inside the sample will not undergo any thermal exchange with the air flow. In fact, the thermal exchange will mainly occur on the surface of the entire sample. Therefore, although heating of compressed powder samples in a microwave is possible, it is difficult to directly heat the aerosols and droplets on contaminated respirators to the deactivation temperature using direct microwave irradiation. However, if a small amount of water is placed beneath the respirator, the microwave could easily heat the water and generate high-temperature steam. This explains why MGS is effective for this form of decontamination.

IV. Conclusion

In this work, the dry microwave heating of ultra-small infectious aerosols or droplets on respirators was systematically investigated. In the process, the microwave absorption performance of an ultra-small water sphere representing an infectious aerosol or droplet was theoretically analyzed, while multiphysics simulation was carried out, with the results indicating that dry microwave heating can barely heat a single aerosol or droplet under thermal convection boundary conditions. We also conducted experiments using a traveling waveguide system, with the results verifying the multiphysics simulation. Following this, we modeled multiple hemispheres on the respirator material to simulate multiple aerosols and droplets. The simulated results indicated that the aerosols/droplets and the respirator were at the same temperature. Experiments involving a N95 respirator heated in a microwave oven for 2 min were then conducted. Here, the final increase of the respirator temperature was less than 10 °C, which is far lower than the required temperature to deactivate the COVID-19 virus. Therefore, we can conclude that dry microwave heating cannot be used to decontaminate respirators for reuse, even though previous results have indicated that dry microwave irradiation does not result in significant degradation of the filtering and fitting of the respirators [11].

However, MGS remains an effective method for decontaminating respirators, as tested and reported in many existing reports [3], [10], [12], [13]. Here, special attention should be paid to the water beneath the respirator. The presence of water (or a steam bag) is of vital importance, and the generated steam should cover the entire respirator, including the straps. Meanwhile, although the volume of water should not be too large, the precise amount is, at present, largely indeterminable because of the variety of microwave oven models and power settings. However, it can be stated that ensuring that water is present during the whole process, with its small amount remaining after the heating, will likely prove to be effective. In future, the multiphysics simulation which includes the entire process of heating a respirator on a water tank in a microwave oven could be studied to help the optimization of disinfection. Experiments involving the filtering performance, the fitting, and the germicidal effect could also be conducted to ascertain the optimal protocols for different microwave models.

REFERENCES

[1] L. Liao *et al.*, "Can N95 respirators be reused after disinfection? How many times," *ACS nano*, vol. 14, no. 5, pp. 6348–6356, 2020.

[2] M. A. Khan, A. Ikram, S. Savul, F. K. Lalani, M. A. Khan, and M. Sarfraz, "Decontamination and reuse of N95 masks: A narrative review," *Can. J. Infectious Diseases Med. Microbiol.*, vol. 2020, pp. 1–9, Nov. 2020.

[3] K. E. Zulauf *et al.*, "Microwave-generated steam decontamination of N95 respirators utilizing universally accessible materials," *mBio*, vol. 11, no. 3, Jun. 2020, Art. no. e00997.

[4] M. Bergman, E. Fisher, and B. Heimbuch, "A review of decontamination methods for filtering facepiece respirators," *J. Int. Soc. Respir. Prot.*, vol. 37, no. 2, pp. 71–86, 2020.

[5] L. Cassorla, "Decontamination and reuse of N95 filtering facepiece respirators: Where do we stand?" *Anesthesia Analgesia*, vol. 132, no. 1, pp. 2–14, 2021.

[6] C. E. Rodriguez-Martinez, M. P. Sossa-Briceño, and J. A. Cortés, "Decontamination and reuse of N95 filtering facemask respirators: A systematic review of the literature," *Amer. J. Infection Control*, vol. 48, no. 12, pp. 1520–1532, Dec. 2020.

[7] J. B. Lynch *et al.*, "Infectious diseases society of America guidelines on infection prevention for healthcare personnel caring for patients with suspected or known coronavirus disease 2019," *Clin. Infectious Diseases*, Jul. 2020.

[8] A. Price *et al.*, "Is the fit of N95 facial masks effected by disinfection? A study of heat and UV disinfection methods using the OSHA protocol fit test," *medRxiv*, Apr. 2020, doi: 10.1101/2020.04.14.20062810.

[9] S. Gertsman *et al.*, "Microwave-and heat-based decontamination of N95 filtering facepiece respirators: A systematic review," *J. Hospital Infection*, vol. 106, no. 3, pp. 536–553, 2020.

[10] E. M. Fisher, J. L. Williams, and R. E. Shaffer, "Evaluation of microwave steam bags for the decontamination of filtering facepiece respirators," *PLoS ONE*, vol. 6, no. 4, Apr. 2011, Art. no. e18585.

[11] D. Viscusi, W. King, and R. Shaffer, "Effect of decontamination on the filtration efficiency of two filtering facepiece respirator models," *J.-Int. Soc. Respiratory Protection*, vol. 6, no. 4, pp. 93–107, 2007.

[12] B. K. Heimbuch *et al.*, "A pandemic influenza preparedness study: Use of energetic methods to decontaminate filtering facepiece respirators contaminated with H1N1 aerosols and droplets," *Amer. J. Infection Control*, vol. 39, no. 1, pp. e1–e9, Feb. 2011.

[13] M. Lore, B. Heimbuch, T. Brown, J. Wander, and S. Hinrichs, "Effectiveness of three decontamination treatments against influenza virus applied to filtering facepiece respirators," *Ann. Occupational Hygiene*, vol. 56, no. 1, pp. 92–101, 2012.

[14] M. Bergman, D. Viscusi, B. Heimbuch, J. Wander, A. Sambol, and R. Shaffer, "Evaluation of multiple (3-cycle) decontamination processing for filtering facepiece respirators," *J. Eng. Fibers Fabrics*, vol. 5, no. 4, pp. 33–41, 2010.

[15] M. Bergman, D. Viscusi, A. Palmiero, J. Powell, and R. Shaffer, "Impact of three cycles of decontamination treatments on filtering facepiece respirator fit," *J. Int. Soc. Respiratory Protection*, vol. 28, no. 1, pp. 48–59, 2011.

[16] M. Moustafa, "Characteristics of biological and non-biological aerosol particles in indoor environment and their inhalable fractions in the human lung," *Arab J. Nucl. Sci. Appl.*, vol. 53, no. 1, pp. 243–251, 2020.

[17] J. Tryner, J. Mehaffy, D. Miller-Lionberg, and J. Volckens, "Effects of aerosol type and simulated aging on performance of low-cost PM sensors," *J. Aerosol Sci.*, vol. 150, Dec. 2020, Art. no. 105654.

[18] W. W. F. Leung and Q. Sun, "Electrostatic charged nanofiber filter for filtering airborne novel coronavirus (COVID-19) and nano-aerosols," *Separat. Purification Technol.*, vol. 250, Nov. 2020, Art. no. 116886.

[19] J. A. Stratton, *Electromagnetic Theory*. Hoboken, NJ, USA: Wiley 2007, pp. 563–573.

[20] T. Yamane, A. Nishikata, and Y. Shimizu, "Resonance suppression of a spherical electromagnetic shielding enclosure by using conductive dielectrics," *IEEE Trans. Electromagn. Compat.*, vol. 42, no. 4, pp. 441–448, Nov. 2000.

[21] S. A. Barringer, E. A. Davis, J. Gordon, K. G. Ayappa, and H. T. Davis, "Effect of sample size on the microwave heating rate: Oil vs. Water," *AIChE J.*, vol. 40, no. 9, pp. 1433–1439, Sep. 1994.

[22] Y. Zhang, D. K. Agrawal, J. Cheng, and T. Slawecki, "Microwave power absorption mechanism of metallic powders," *IEEE Trans. Microw. Theory Techn.*, vol. 66, no. 5, pp. 2107–2115, May 2018.

[23] R. Roy, D. Agrawal, J. Cheng, and S. Gedevanishvili, "Full sintering of powdered-metal bodies in a microwave field," *Nature*, vol. 399, no. 6737, pp. 668–670, Jun. 1999.

[24] J. Cheng, R. Roy, and D. Agrawal, "Experimental proof of major role of magnetic field losses in microwave heating of metal and metallic composites," *J. Mater. Sci. Lett*, vol. 20, no. 17, pp. 1561–1564, 2001.

[25] D. N. Gamit and M. K. Chudasama, "Size-effect in microwave processing of engineering materials—A review," *J. Mech. Eng. Sci.*, vol. 14, no. 2, pp. 6770–6788, Jun. 2020.

[26] O. M. Kesbi, A. Rajabipour, M. Omid, and S. H. Goldansaz, "Determination of electric field intensity during microwave heating of selected vegetables and fruits," *J. Microw. Power Electromagn. Energy*, vol. 52, no. 4, pp. 276–286, Oct. 2018.

[27] K. Pitchai, S. L. Birla, J. Subbiah, D. Jones, and H. Thippareddi, "Coupled electromagnetic and heat transfer model for microwave heating in domestic ovens," *J. Food Eng.*, vol. 112, nos. 1–2, pp. 100–111, Sep. 2012.

[28] R. Grainger, J. Lucas, G. Thomas, and G. Ewen, "Calculation of Mie derivatives," *Appl. Opt.*, vol. 43, no. 28, pp. 5386–5393, 2004.

[29] X. Zhao, L. Yan, and K. Huang, "Review of numerical simulation of microwave heating process," in *Advances in Induction and Microwave Heating of Mineral and Organic Materials*. Rijeka, Croatia: InTech, 2011, pp. 27–48.

[30] H. Moosmüller and W. P. Arnott, "Particle optics in the Rayleigh regime," *J. Air Waste Manage. Assoc.*, vol. 59, no. 9, pp. 1028–1031, Sep. 2009.

[31] P. Kosky, R. Balmer, W. Keat, and G. Wise, *Exploring Engineering, An Introduction to Engineering and Design*, 3rd ed. Salt Lake City, UT USA: Elsevier, 2012, pp. 259–281.

[32] S. Erlandsson, "Evaluation, adaption and implementations of perfectly matched layers in COMSOL multiphysics," Ph.D. dissertation, School Eng. Sci., KTH Royl Inst. Technol., Stockholm, Sweden, 2020.

[33] E. Grant and B. Halstead, "Dielectric parameters relevant to microwave dielectric heating," *Chem. Soc. Rev.*, vol. 27, no. 3, pp. 213–224, 1998.

[34] A. Alfraihat, "Study of permittivity of saliva and urine to classify different stages of breast carcinoma," Ph.D. dissertation, Dept. Eng., Univ. Malaya, Kuala Lumpur, Malaysia, 2011.

[35] R. Somaraju and J. Trumpf, "Frequency, temperature and salinity variation of the permittivity of seawater," *IEEE Trans. Antennas Propag.*, vol. 54, no. 11, pp. 3441–3448, Nov. 2006.

[36] D. F. Li, J. L. Cadnum, S. N. Redmond, L. D. Jones, and C. J. Donskey, "It's not the heat, it's the humidity: Effectiveness of a Rice cooker-steamer for decontamination of cloth and surgical face masks and N95 respirators," *Amer. J. Infection Control*, vol. 48, no. 7, pp. 854–855, Jul. 2020.

[37] M. J. Pascoe *et al.*, "Dry heat and microwave-generated steam protocols for the rapid decontamination of respiratory personal protective equipment in response to COVID-19-related shortages," *J. Hospital Infection*, vol. 106, no. 1, pp. 10–19, Sep. 2020.

[38] J. Ma *et al.*, "Systematic study of microwave absorption, heating, and microstructure evolution of porous copper powder metal compacts," *J. Appl. Phys.*, vol. 101, no. 7, Apr. 2007, Art. no. 074906.

Kama Huang (Senior Member, IEEEE) received the M.S. and Ph.D. degrees in microwave theory and technology from the University of Electronic Science and Technology, Chengdu, China, in 1988 and 1991, respectively.

He joined the National Research Council of Italy (CNR), Genoa, Italy, in 1997; Technical University Vienna, Vienna, Austria; in 1999; and Clemson University, Clemson, SC, USA, in 2001, as a Visiting Scientist. He has been a Professor with the Department of Radio and Electronics, Sichuan University, Chengdu, China, since 1994, and he was the Director of the department from 1997 to 2017. His research interests lie in the areas of microwave chemistry and electromagnetic theory.

Junjun Li, photograph and biography not available at the time of publication.

Yi Zhang (Member, IEEE), photograph and biography not available at the time of publication.